

PERMAFROST MODEL IN COARSE-BLOCKY DEPOSITS FOR THE DRY ANDES, ARGENTINA (28°-33° S)¹

C. TAPIA BALDIS*, D. TROMBOTTO LIAUDAT

IANIGLA (Instituto Argentino de Nivología, Glaciología y Ciencias Ambientales), CCT Conicet Mendoza, Argentina

ABSTRACT. *In this work, a statistical permafrost distribution model for coarse-blocky deposits in the Dry Andes of Argentina (28-33°S) is presented. The empiric mathematical formulation was based on a logistic regression. The final model is a combination of two independent occurrence probability models: a) a mean annual air temperature-terrain ruggedness model and, b) a mean annual air temperature-potential incoming solar radiation model. For all cases, calibration was made according the complete geomorphological characterization of a periglacial basin with 250 km². Lately, the results of probabilistic model were extrapolated to the whole study area in the Dry Andes and compared with the Argentine rock glacier inventory data base. High permafrost likelihood, in coarse debris, is expected above 4200 and 5700 m a.s.l., from south to north in the study area and covers a surface of approximately 1200 km². Medium permafrost likelihood is expected above 3400 and 4200 m a.s.l. with a surface of 6178 km² while low permafrost likelihood, occurs between 3000 and 3400 m a.s.l. with an area of 11.060 km². These findings indicate that permafrost may occur in several types of coarse-blocky deposits in the Dry Andes, not only restricted to rock glaciers. Thermal properties of the ground in coarse-blocky deposits allow permafrost permanence, even under unfavourable climatic conditions.*

The performance of the permafrost model was also tested, considering the transition from cold paleoclimate Tardiglacial to present climatic conditions. During the warming, likely permafrost surface reduced from 56 to 13%. In the same way, rock glaciers with high and medium permafrost likelihood decrease from 62 to 30%, respectively while, rock glaciers with low likelihood and no permafrost category, increased 75% and 474%, respectively. Moreover, we identified some sites in which permafrost degradation is arguably expected. About that, 0.9% of

¹ This paper has received the First Prize and Honorable Mention (shared) from the Young Researcher Innovation Award on Cryosphere Science, granted by the Research Group on Physical Geography in High Mountains, Complutense University of Madrid (Department of Geography), Spain.

the rock glaciers in the study area display possible permafrost degradation and 33% of them, likely permafrost degradation.

Modelo de permafrost en depósitos detríticos gruesos para los Andes Secos de Argentina (28-33° S)

RESUMEN. *En este trabajo se exponen los resultados de un modelo probabilístico de presencia de permafrost en depósitos detríticos gruesos para un sector de los Andes Secos de Argentina (28-33°S). La formulación matemática responde a un modelo de regresión logística. El modelo final es el resultado combinado de dos modelos probabilísticos independientes de permafrost: a) el modelo de temperatura media anual del aire – rugosidad del terreno y b) el modelo de temperatura media anual del aire – radiación solar potencial entrante. En todos los casos, la calibración se realizó de acuerdo a la completa caracterización geomorfológica de una cuenca periglacial de 250 km². Posteriormente, los resultados del modelo probabilístico fueron extrapolados para toda la región de estudio en los Andes Secos y comparado con los datos recientemente publicados del inventario de glaciares rocosos (o glaciares de escombros, en Sudamérica) de Argentina.*

Sobre 4200 a 5700 m snm, de sur a norte del área de estudio, existen altas probabilidades de encontrar permafrost en depósitos detríticos gruesos, cubriendo un área de 1200 km². Por sobre 3400 y 4200 m snm, las probabilidades de encontrar permafrost en este tipo de depósitos son medias, en una superficie de 6178 km² mientras que, entre 3000 y 3400 m snm, su presencia es poco probable y la superficie correspondiente es de 11.060 km². Estos resultados reflejan que el permafrost puede estar presente no sólo en glaciares rocosos. Las propiedades térmicas del suelo en las cubiertas detríticas gruesas son las que permiten su permanencia, incluso bajo condiciones ambientales desfavorables.

Se comparó también la respuesta de nuestro modelo frente a la transición de un paleoclima Tardiglacial más frío hasta el clima presente. Durante el calentamiento, la superficie posiblemente ocupada por permafrost experimentó una reducción del 56 al 13%. Del mismo modo, los glaciares rocosos con alta y media probabilidad de permafrost disminuyeron entre 62% y 30%, respectivamente. Por otro lado, los glaciares rocosos afectados con permafrost poco probable y posiblemente ausente, se incrementaron del 75% al 474%. Además, identificamos sectores en los que es posible se produzcan fenómenos de degradación de permafrost. Al respecto 0.9% de los glaciares rocosos del área de estudio poseen permafrost con altas probabilidades de degradación y 33%, con posibilidades medias de degradación.

Key words: Mountain permafrost, Dry Andes, Argentina, Logistic regression model.

Palabras clave: Permafrost de montaña, Andes Secos, Argentina, modelo de regresión logística.

Received: 30 October 2018

Accepted: 14 February 2019

*Corresponding Author: Carla Tapia Baldis. IANIGLA (Instituto Argentino de Nivología, Glaciología y Ciencias Ambientales), CCT Conicet, Av. Ruiz Leal s/n. Parque Gral. San Martín. CP: 5500. CC: 330, Mendoza, Argentina. E-mail address: ctapia@mendoza-conicet.gob.ar

1. Introduction

The Dry Andes of Argentina contain extensive areas currently with permafrost condition. The term permafrost is used to identify rock or ground (soil or rock, including ice and/or organic material) that remains at or below 0°C for at least two consecutive years (van Everdingen, 1998). As permafrost is a temporary-thermal phenomenon thus, not directly visible, its recognition and quantification are challenging, especially in a complex high-mountain topography, where its natural extension is discontinuous or in patches. Its occurrence is controlled by regional and local scale interactions between climatic patterns, topographic features, surface and ground properties (Gruber and Haeberli, 2009).

Traditionally, rock glaciers are widely used as mountain and Andean permafrost indicators (Haeberli, 1985; Barsch, 1996; Humlum, 1996; Trombotto, 2000; Harris *et al.*, 2009; Haeberli *et al.*, 2010; Saito *et al.*, 2016). Rock glaciers are mesoscale landforms built-up by masses of rock fragments and finer material that, if active, move down slope by influence of gravity through a creeping mechanism, involving ground ice deformation (Barsch, 1996; Trombotto *et al.*, 2014). According to the recently published Argentine rock glacier inventory (IANIGLA, 2017), more than 600 km² of national territory is occupied by active and inactive rock glaciers (6846 landforms >1 km²), both indicating old or current creeping permafrost conditions. However, rock glacier surface alone underestimates the real extension of permafrost in cold high-mountain environments. Mountain permafrost can also be found below several surface-types: under perennial snow covers, in steep bedrock, fine or coarse talus slopes or deposits, or in valley bottoms (Boeckli *et al.*, 2012; Scherler, 2014).

High altitude and cold climate settings allowed permafrost to develop and persist over the time, but in last instance, local surface and ground-surface characteristics, with specific thermal properties, determine permafrost occurrence under non-favourable climatic conditions. Several authors (Trombotto *et al.*, 1997, 1999; Azócar and Brenning, 2010; Martini *et al.*, 2013; Azócar *et al.*, 2017; Tapia Baldis, 2018) noted that, in the Andes of Argentina and Chile, rock glacier's terminus commonly lie at or below the 0°C mean annual air (MAAT) temperature. According to Haeberli *et al.* (2010) and Gruber and Hoelzle (2008), coarse-blocky surfaces, which typically exist on rock glacier surfaces, may have a cooling influence on the ground, based on temperature-driven air convection. This effect is further enhanced or inhibited by the thickness and duration of the snow cover.

In coarse debris or blocky surfaces convective and radiative heat-transfer mechanisms prevail over conductive ones, due to the small inter-connections in the rock matrix (Johansen, 1975). Balch effect (Balch, 1900; Barsch, 1996) and chimney effect (Delaloye *et al.*, 2003) are examples of convective circulation inside blocky surfaces due to air density differences and can occur over flat or slope scree surfaces (Delaloye *et al.*, 2003; Wicky and Hauck, 2017). Semi-conductive behaviour of blocky deposits (Gruber and Hoelzle, 2008) and high insulating characteristics due to the low conductivity of air in the voids (Juliussen and Humlum, 2008), may lead to the existence of permafrost at places where, without such covertures, it would not develop (Delaloye *et al.*, 2003; Scherler *et al.*, 2014; Wicki and Hauck, 2017). Besides, temperature-driven seasonal subsurface ventilation through layers of coarse blocks on steep slopes can locally reduce mean ground temperatures by several degrees °C (Delaloye and Lambiel, 2005).

Due to the extensive presence of coarse-blocky deposits and fine sedimentary accumulations in the study area (*ca.* 55% coarse-debris accumulations, 30% fine sedimentary deposits and 15% of steep bedrock outcrops), an empiric-static model to estimate regional mountain permafrost distribution over these kinds of surfaces, beyond the rock glacier's domain, was developed. As Boeckli *et al.* (2012) suggested, permafrost distribution models should distinguish between surface characteristics to avoid the extrapolation of permafrost classes over different covers. We opted for a logistic regression model, previously used by several authors (Brenning and Trombotto, 2006; Azócar *et al.*, 2017). Permafrost predictive variables are the MAAT at the air-ground interphase, potential incoming solar radiation (PISR) and terrain ruggedness index (TRI), as offset to distinguish between steep bedrock and sedimentary (coarse and fine) accumulations. The complete geomorphological characterization of the Bramadero river basin, chosen as calibration area, and the geomorphometric data from every single kind of landform, were used to set up the permafrost predictive categories.

2. Study area

The study area (28° to 33°S and 70°30' to 69°W) comprises the middle portion of the South American (Argentinian side) Central Andes (17°30' to 35°S), named Dry Andes (Lilboutry, 1998) (Fig. 1a). The landscape is expressed as mountain ranges and valleys with 50% of terrain surface above 3000 m a.s.l. The highest elevations are represented by mountain peaks such as Mercedario (6850 m a.s.l.) or La Ramada (6400 m a.s.l.). Dry Andes could be further separated into Desert Andes (17°30' to 31°S) and Central Andes (31° to 35°S), according precipitation rates and landscape geomorphological characteristics (Lilboutry, 1998).

Tectonically, the study area is placed on the flat-slab portion from the Nazca tectonic plate (27° to 33°30'). This segment is characterized by intense seismic activity (Isacks *et al.*, 1982), expressed through active faults and the development of an orogenic front that involves Quaternary units (Ramos *et al.*, 1997) and, no volcanic activity since *ca.* 25 Myr (Jordan *et al.*, 1983). More than 60 lithological units and complexes are currently recognized involving intrusive, effusive, volcanoclastic and sedimentary rock types, with ages ranging up to 360 Myr.

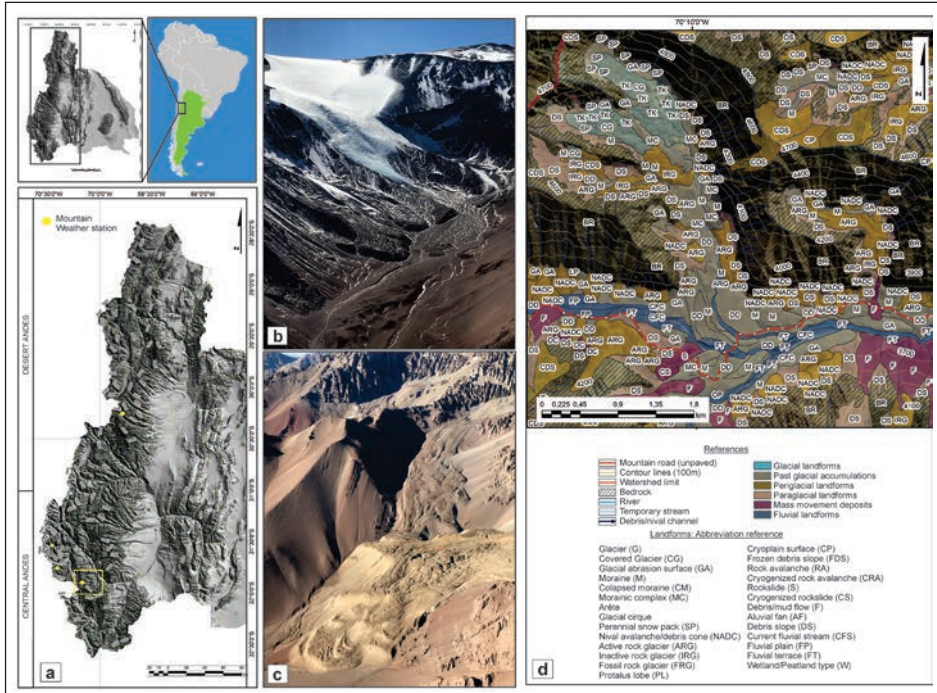


Figure 1. a) Regional context of the study area (Dry Andes of Argentina). Yellow square delimits calibration area for permafrost occurrence models. b) Glacial landscape in the Desert Andes at ca. 4700 m a.s.l. (Photo: D. Trombotto, 2018). c) Periglacial landscape in the Central Andes, showing typical coarse-blocky debris accumulation on rock glaciers (Photo: D. Trombotto, 2018). d) Example of geomorphological classification in Bramadero river basin (calibration area). Landform-type, abbreviation and landscape system are detailed in figure. Base figure: ALOS-PRISM imagery.

Data for model calibration was obtained from the Bramadero river basin, located at 31°50' S and 70°00' W in the Central Andes (Fig. 1a). Climatic conditions in the region show a well-defined seasonal regime with maximum nival precipitation (300-400 mm/yr) during the cold season (April-October) and scarce nival precipitation during the warm season (November-March). Snow cover does not remain after the cold season outside topographically protected snow niches, over 4500 m a.s.l. Moreover, the precipitation is strongly controlled by the phase of El Niño Southern Oscillation (ENSO) (Montecinos and Aceituno, 2003), with annual means of 60-70 mm during La Niña phases and annual maximums of 1100-1200 mm during El Niño wetter phases. A weather station placed on the bottom of the main valley recorded a MAAT of -2.15°C between 2009-2014 at a height of 4019 m a.s.l.

From a geomorphological point of view, the landscape of the Dry Andes is characterized by the interdigitation of glacial, periglacial, alluvial, fluvial and gravitational processes (Figs. 1b and 1c). The last glacial maximum ice extent is believed to have

occurred *ca.* 40 kyr BP in this region, prior to the global Last Glacial Maximum (LGM), as a result of increased winter precipitation due to a stronger influence of Southern Westerlies (Zech *et al.*, 2017). The Bramadero river basin was largely glaciated during the LGM, even today it is possible to recognize erosive forms and glacial deposits all over the main valley and subordinated creeks. Even though Quaternary glacial stages modelled the landscape; periglacial features prevail today. Currently, periglacial processes are active in elevations exceeding 2700 m a.s.l. (lowest limit of seasonal freezing), however, a wide variety of periglacial deposits and permafrost indicating cryoforms occur between 3400 and >4500 m a.s.l. (permafrost periglacial belt) (Tapia Baldis, 2018). As a result of active tectonic processes and secondary mineralization alteration, glacial and periglacial over imposed denudation processes, active frost-weathering action, reduced or almost inexistent perennial snow cover and lack of vegetation, only 10% of the Dry Andean surface represents steep sediment-free bedrock.

3. Methods and data

3.1. Permafrost modelling

In order to predict regional-scale spatial patterns of permafrost occurrence, especially over remote environments with limited data, empiric-statistical models are widely used (Riseborough *et al.*, 2008; Sattler *et al.*, 2016; Deluigi *et al.*, 2017; Marcer *et al.*, 2017; Zhao *et al.*, 2017; Zou *et al.*, 2017). This kind of approaches correlates permafrost occurrence with topo-climatic factors (altitude, geographic position, slope, aspect, air temperature, ground temperature, solar radiation, etc.) easily available, in some cases. Different combinations of empiric-statistical models were tested to evaluate the permafrost spatial distribution in the study area. Models were trained in a calibration area to evaluate the correlation between geomorphological permafrost indicators (named explanatory variable) and the topoclimatic parameters (predictive variable). A logistic regression model with a logit link function was chosen as mathematical approach (Brenning and Trombotto, 2006; Boeckli *et al.*, 2012; Azócar *et al.*, 2017; Marcer *et al.*, 2017).

Model goodness of fitting, was performed through the Hosmer-Lemeshow test (2000); while regression contrast was made by the Verisimilitude function. The Akaike Information Criterion (Akaike, 1974) was used to compare the fitting quality of different models, penalizing the overfitting achieved by complex models. In all cases, p-value was 0.001.

Regional-patterns of permafrost occurrence were computed in ArcGIS with *raster calculator*, using the regression coefficients obtained for each model. Results were cross-validated with the Argentine rock glacier inventory (IANIGLA, 2017) and with field work inspections.

Permafrost probability values were converted into likelihood of occurrence indexes, through common off-sets, according to the suggestions of Boeckli *et al.* (2012); Gruber (2012); Azócar *et al.* (2017) and Marcer *et al.* (2017). Selected thresholds are:

- High permafrost likelihood ($P > 75\%$): permafrost over coarse-blocky deposits in all kind of environmental conditions.

- Medium permafrost likelihood ($75\% > P > 50\%$): permafrost over coarse-blocky deposits in cold favourable climatic conditions.
- Low permafrost likelihood ($50\% < P < 25\%$): permafrost over coarse-blocky surfaces with unfavourable climatic conditions. Landforms in local cold microclimates or topographically protected zones; may also indicate spatial patterns of relict or degraded permafrost.
- No permafrost ($P < 25\%$): under current climatic conditions, no permafrost should be expected below coarse-blocky deposits. Permafrost may occur at exceptional sites such as cold caves or in dead-ice.

3.2. Logistic Regression Model

Logistic regression is a mathematical modelling approach that can be used to describe the relationship of several independent variables to the dichotomously dependent one (Kleinbaum and Klein, 2010). This model allows the use of quantitative or categorical independent variables (also named explanatory variables), which do not necessarily adopt a normal distribution, to predict the probability of a phenomenon. In our case, the logistic distribution function $[P(x)]$ represents the probability P of permafrost presence or absence due to independent environmental and topographical variables (X_i), defined as follows (Equation 1).

$$P(x) = \left[\frac{1}{1+e^{-z}} \right]; \text{ and } Z = \beta_0 + \sum_{i=1}^n \beta_i X_i \quad (\text{Equation 1})$$

An alternative way to express the logistic model is by the logit or Z form. The logit transformation modifies the logistic formula into a simpler linear one as (Equation 2):

$$\text{Logit} = \left[\frac{e^x}{1+e^x} \right] = \ln \left[\frac{P}{1-P} \right] = Z = \beta_0 + \sum_{i=1}^n \beta_i X_i \quad (\text{Equation 2})$$

The β_i values are coefficients measuring how each one of the explanatory variables (X_i) contributes to the permafrost presence while β_0 represents the baseline permafrost odds.

The logit formulation acts showing the equivalence between permafrost probabilities derived from explanatory continuous variables, and its presence/absence as a binary one (Boeckli *et al.*, 2012).

3.3. Geomorphological mapping and permafrost evidences

Permafrost presence is usually established from geomorphological indicators, geophysical or thermal data (surface or borehole data) (Barsch, 1996; Trombotto and Borzotta, 2009). Rock glaciers and protalus ramparts are widely used as creeping-permafrost indicators (Trombotto, 2003). According to Barsch (1996), active and

inactive forms indicate the presence of permafrost, but they differ in the rates of creeping by ice-deformation and therefore, in their movement rates. Relict or fossil rock glaciers denote permafrost and ground-ice absence (Trombotto, 2003). Measuring of rock glacier dynamics was not able when this study was performed, but was recently presented by Villarroel *et al.* (2018), while data regarding active layer status are scarce or almost non-existent. However, another kind of landforms may have *in situ* permafrost (stationary, not creeping) or, may have mountain permafrost, and ground-ice, but are not reliable geomorphological indicators (Trombotto, 1991). At the moment, resistivity and geoelectric measurements to detect frozen materials are also very few (Croce and Milana, 2002; Arenson *et al.*, 2010).

The complete geomorphological characterization of the Bramadero river basin, chosen as calibration area, and the geomorphometric data extracted from every kind of landform, were used to set up the permafrost predictive categories. Landforms and processes were mapped from ALOS PRISM imagery (Panchromatic Remote-Sensing Instruments for Stereo Mapping). We used a topographic base from the 45 m resolution digital elevation model provided by the Argentine Geographic Institute (henceforth AR-DEM). Figure 1d displays an example of geomorphological features in the calibration basin.

The first predictive category (presence) includes geoforms that certainly indicate current permafrost, such as; active rock glaciers, inactive rock glaciers, protalus lobes, cryoplanation surfaces and perennial snow patches. The second category (absence) includes geoforms without current permafrost (relict or fossil rock glaciers, bedrock outcrops, glacial abrasion surfaces, debris/mud flows and Andean wetlands/peatlands types). It also includes geoforms where the presence of permafrost could not be certainly assessed such as: frozen and unfrozen talus slopes, glaciers and covered glaciers, moraines and morainic complexes, debris/snow avalanches, rock avalanches and rock slides.

3.4. Explanatory variables

3.4.1. Mean Annual Air Temperature (MAAT; 1979-2010)

The MAAT was modelled using the period gridded data from NCEP-CSFR reanalysis series from 1979 to 2010 (Saha *et al.*, 2010). Monthly and yearly were compared with the available - yet scarce data - from five local mountain meteorological stations (three placed in the Central Andes and two in the Desert Andes, see Figure 1a) with standard deviations (SD), root-mean-square deviation (RMSD), root-mean-square error (RMSE) and mean-absolute percentual error (MAPE). The NCEP-CSFR data provides the temperature in the contact interphase between ground-atmosphere (at 2 m above the ground), gridded at 0.5° spatial resolution, also named surficial air temperature (Cao *et al.*, 2017). Since MAAT strongly varies latitudinally and altitudinally through the study area, a downscaled model was made, using a simple lapse rate (-6.5°C/1000 m). The small number and uneven spatial distribution of weather stations inhibited the local lapse rate calculation and the MAAT modeling from *in situ* measurements.

3.4.2. Potential Incoming Solar Radiation (PISR)

PISR was calculated in SAGA GIS® with the *Terrain Analysis* tool, using the AR-DEM, a time-lapse of 1 hour every 5 days during one year; annual values were then averaged for the period 1979-2010. PISR comprehend the sum of direct and diffuse solar radiation. Yearly values of PISR were compares with solar radiation registers from “*Portezuelo de la Guardia*” meteorological station (PG; Unidad de Geocriología, 2009-2014), placed inside the calibration area at 4019 m a.s.l.

3.4.3. Terrain Ruggedness Index (TRI)

Terrain Ruggedness Index (Ryley *et al.*, 1999) is an expression that quantifies the roughness of the surface through considerations of absolute elevations in the surrounding of a given raster cell. TRI is expressed as (Equation 3):

$$TRI = (\sum(Zc - Zi)^2)^2 \quad (\text{Equation 3})$$

where ZC is the elevation of a given central raster cell and Zi is the elevation of one of the eight neighbouring cells (with i ranging from 1 to 8). TRI values were obtained using the homonymous algorithm in SAGA GIS® from the AR-DEM. Manual calibration of TRI indexes allowed the discrimination of steep bedrock outcrops ($TRI > 19-20$), coarse-debris deposits ($19 > TRI > 5$) and flat surfaces with fine sedimentary accumulations ($TRI < 5$).

3.5. Paleoclimatic scenarios and spatial patterns of permafrost degradation

A later step in our work was to compare the permafrost occurrence between past and present climatic scenarios. We tested the performance of the final permafrost distribution model (section 4.2) over a “cold climatic scenario”, where hypothetically, the current MAAT-5°C may respond, to the paleoclimatic conditions in the study area (section 5.2). Expected permafrost occurrences under present climatic scenario were subtracted to the cold climatic scenario, in order to obtain the probabilistic values of permafrost variation. Similar approach was used by Hoelzle and Haeberli (1995). Moreover, two oversimplification were used: terrain configuration, thus TRI values and distribution, and PISR remain constant and equal to actual conditions. Areas with a reduction in probabilistic values for permafrost occurrence since from cold to present climatic scenarios were considered in this work as: likely degraded permafrost (P reduction < 50%) and possible degraded permafrost (P reduction < 25%).

4. Results

4.1. Geomorphological mapping in the calibration area

Based on the geomorphological characterization of the Bramadero river basin, contrasted with field observations (Fig. 1d), 2344 landforms were identified. About 34% of the total surface (ca. 80 km²) is occupied by bedrock, while 66% (160 km²) exhibits geoforms resulting from active and inactive geomorphological processes. MAAT values in

the calibration area, averaged for the 1979-2010 period, ranged from -17° to 8.5°C , with a mean of -1.6°C and SD of 4°C . PISR values in the calibration area, averaged for the 1979-2010 period, ranged from 300 to 1360 W/m^2 , with a mean of 900 W/m^2 and SD of 320 W/m^2 . TRI values in the calibration area ranged from 1 to 93, with a mean of 16 and SD of 7.

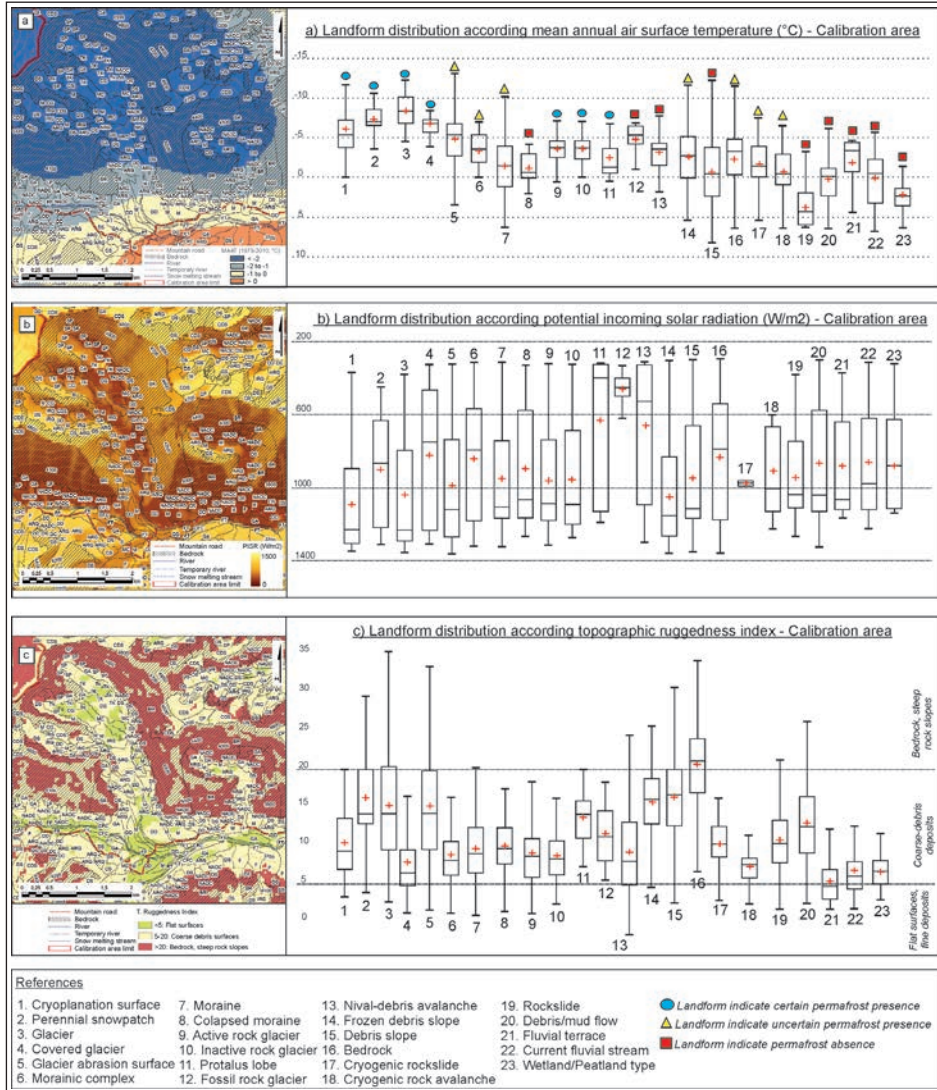


Figure 2. Distribution of explanatory variables for permafrost occurrence in coarse-blocky surfaces in the calibration area. Box-plots represent 75% and whiskers 97% of data, respectively. Red crosses are the mean value. a) MAAT distribution by landforms type (and potential use as permafrost indicator), b) PISR distribution by landform type and, c) TRI distribution according to landform type (fine deposits, coarse-blocky surfaces and steep slope bedrock outcrops are distinguished).

More than 7600 points (94% and 6% corresponding to permafrost absence and presence, respectively) were regularly distributed in the calibration area and used to extract values of MAAT, PISR and TRI in each landform type. Creeping permafrost landforms (rock glaciers, protalus rampart and lobes) reach values from appr. -8°C to slightly positive MAATs at their fronts, while *in situ* permafrost landforms and cold-base glaciers develop only with negative MAATs. Landforms indicating uncertain permafrost presence develop under a wider spectrum of MAATs (Fig. 2a). Neither significant PISR differences according to landform-type, nor differences between PISR values in bedrock and coarse-rocky surfaces were observed, with the exception of fossil rock glaciers with $\text{PISR} < 600 \text{ W/m}^2$ and cryogenic rockslides with PISR appr. 1000 W/m^2 . These constrained ranges are explained by the limited number of such kind of landforms in the calibration area (Fig. 2b). As the water bodies also display TRI values below 5, no previous masking process is needed (Fig. 2c). Mass movement deposits, debris slopes and hanging snow patches may sometimes display high TRI values, as well as rocky outcrops inside some glaciers.

4.2. Statistical Modelling and regional extrapolation

Statistical analysis was based on a dataset of 7462 points and three logistic models compared. A summary of the modeling results for the calibration area is shown in Table 1. The first model, named MAAT-TRI, correctly displays the differences between coarse debris surfaces and bedrock; while the MAAT-PISR model, reflects more precisely temperature ranges for permafrost occurrence in the area, even though it overestimates its extension. Combining both models, realistic results in terms of permafrost distribution patterns and temperature trends were achieved (coarse-blocky deposits permafrost model: CBDP). With AUROC values of 0.75 and 0.84, the performance of all the models used for CBDP generation, can be classified as “very good” according to Hosmer-Lemeshow (2000). Correctly predicted permafrost presence (Sensitivity) and correctly predicted permafrost absence (Specificity), were higher in the MAAT-TRI model than in MAAT-PISR model, due to the restriction of coarse-blocky deposits implicit in the first one. CBDP outstands predicting permafrost presence.

Achieved results from the calibration area were extrapolated to the regional domain of the Dry Andes under study. Table 2 summarizes the results of CBDP model for the Dry Andes showing surface according permafrost probabilistic index, lower altitudinal limit from south to north and corresponding MAATs. Figure 3 displays two examples of extrapolated CBDP model in the Dry Andes. The patterns of permafrost occurrence are shown for coarse-blocky surfaces, as well as likely permafrost degradation patterns.

4.3. Comparison with the PZI model

The CBDP model was compared with the widely accepted permafrost zonation index model (PZI: Gruber, 2012) (Fig. 4). PZI represents spatial patterns of permafrost according favourability regions and includes a fringe of uncertainty that could be included under conservative scenarios. Predictive variables for the PZI are the MAAT (1961-1990) based on the CRU 2.0 and NCEP reanalysis models and the terrain ruggedness index. In

Table 1. Summary of statistics for the logistic models in the calibration area. Explained variability, sensitivity (correctly predicted permafrost occurrence), specificity (correctly predicted permafrost absence) and validation for each model of permafrost occurrence are included as well.

	MAAT-TRI Model	MAAT-PISR Model	CBDP Model
Intercept	-1.87	-1.04	-1.29
MAAT	-0.25	-0.21	-0.19
PISR	-	-0.00052	-0.00042
TRI	-0.20	-	-0.187
Trained AUROC	0.84	0.75	0.84
Explained variability	90%	85%	86%
Sensitivity	83.56%	68.19%	99.88%
Specificity	74.23%	59.71%	0.52%
Observations	7462	7462	7462

Table 2. CBDP model results for the Dry Andes of Argentina, between 29° to 32°S and 70° to 69°30'W. Permafrost occurrence is expressed by likelihood indexes from section 3.1. Lower altitude (m a.s.l.) and MAAT (°C) values range from southern to northern altitudes.

Permafrost Occurrence	Characteristics	Surface (km ²)	Lower Altitude (m a.s.l.)	MAAT (°C)
High likelihood	Permafrost under all environmental conditions	1200	4200 to 5700	-3 to -8
Medium likelihood	Permafrost only under favourable environmental conditions	6178	3400 to 4200	-8 to 1.5
Low likelihood	Permafrost only under highly favourable environmental conditions. Likely degraded permafrost and/or paleo-permafrost.	11 060	3000 to 3400	>1.5

the PZI model, high permafrost likelihood is spreading between 4500 and 5100 m a.s.l. (corresponding MAAT of -18° to -4°C); medium permafrost likelihood between 4000 and 4500 m a.s.l. (MAAT from -10° to -2°C) and low permafrost likelihood between 3700 and 4000 m a.s.l. (MAAT from -7° to 0°C). On the other hand, in the CBDP model high permafrost likelihood is expected between 5700 to 4200 m a.s.l. (MAAT from -18° to -3°C); medium permafrost likelihood between 4200 to 3400 m a.s.l. (MAAT from -8° to 1.5°C) and low permafrost likelihood between 3400 and 3000 m a.s.l. (MAAT from -7° to 5°C).

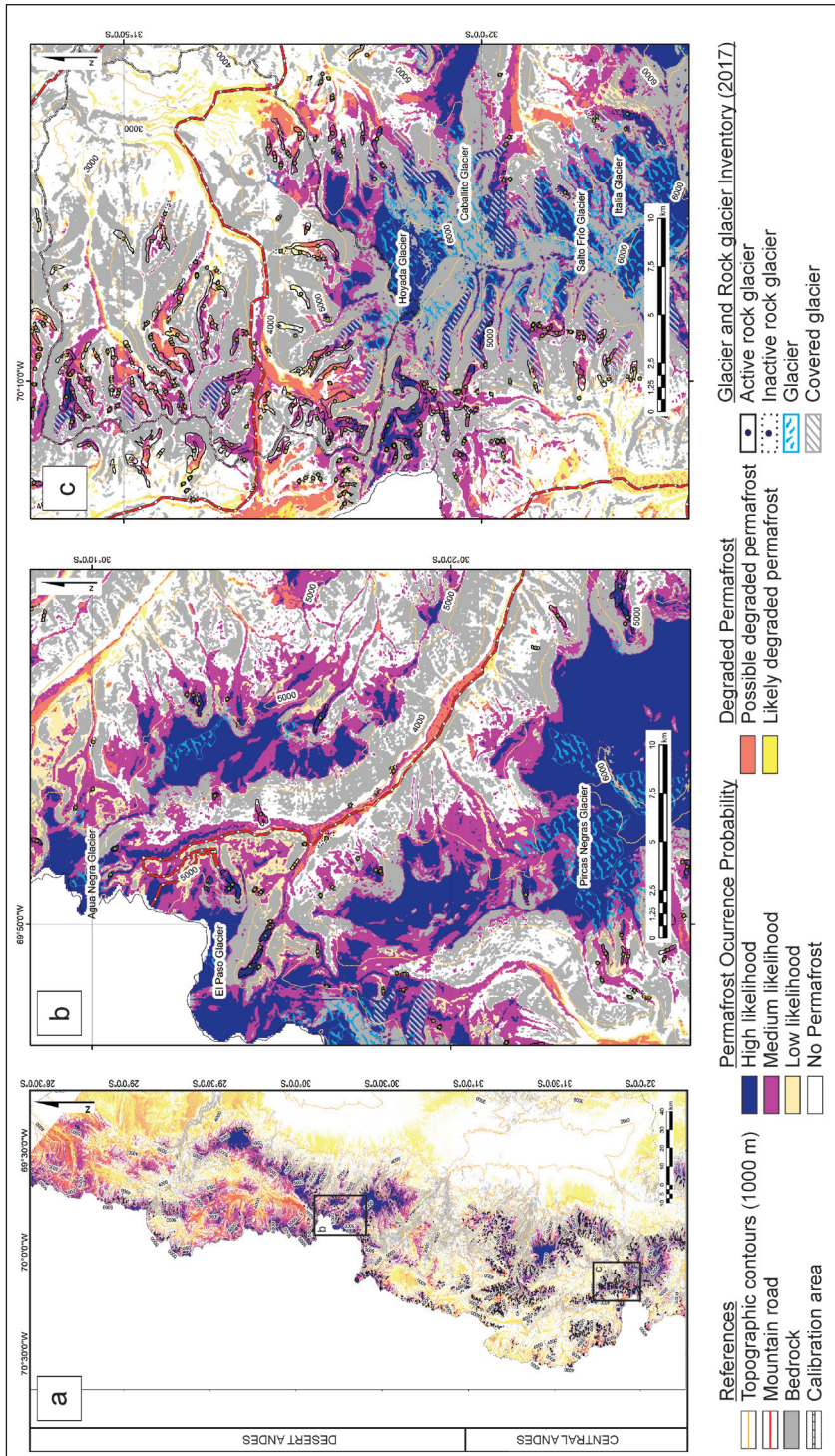


Figure 3. a) Regional extension of CBPF model. Glaciers and rock glaciers from IANIGLA (2017) are included in detail rectangles. b) Permafrost occurrence model according to the CBDP model in the Desert Andes, including the area of "Agua Negra" border pass and projected international tunnel; c) permafrost occurrence model according to the CBDP model in the Central Andes, including the area of "La Ramada" mountain range and Mercedario peak.

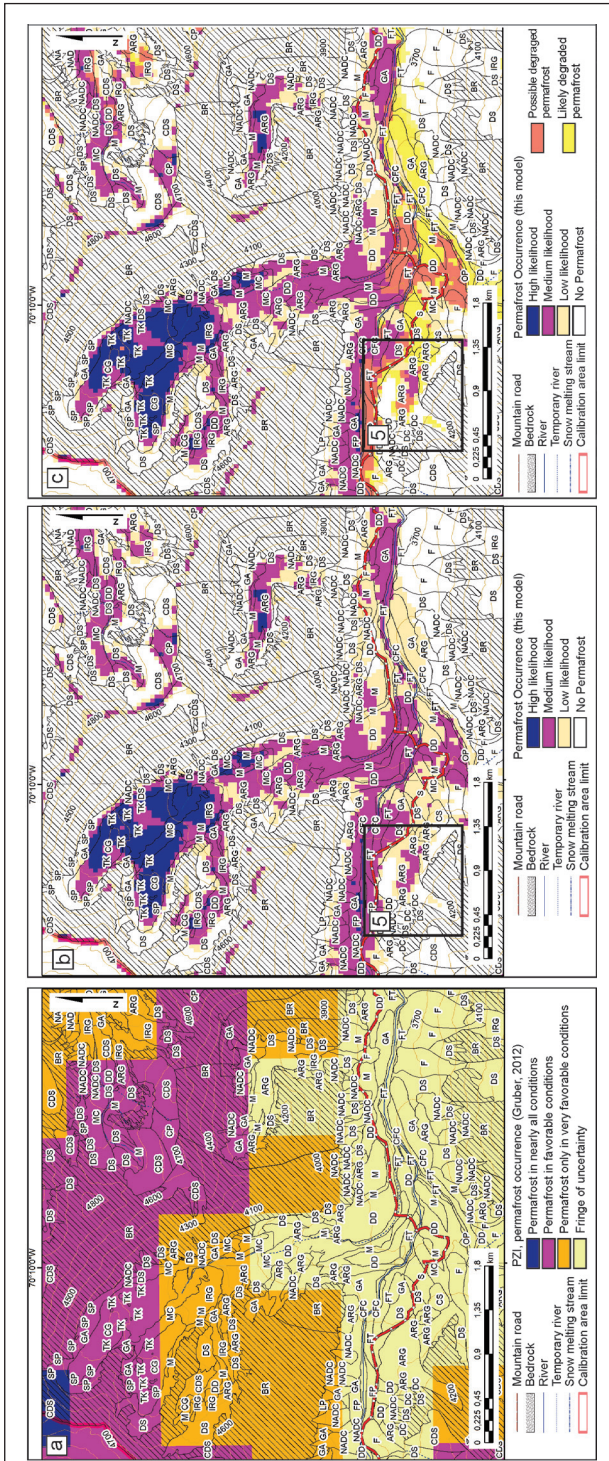


Figure 4. a) PZI permafrost model expression in the calibration area. b) CBBP model performance in the calibration area, under current climatic conditions (1969-2010). c) CBBP model performance with likely permafrost degradation patterns since Tardiglacial (see section 5.3). Grey areas in b) and c) represent bedrock, not included in the permafrost model. Black rectangle shown in figure 5a.

4.4. Paleoclimatic scenarios and spatial patterns of permafrost degradation

Table 3 displays the differences in permafrost altitudes under the present and cold climatic scenarios. Cold climatic scenario not only exhibits both altitudinal and spatial, permafrost wider extension but also, higher permafrost occurrence indexes over coarse-debris deposits. In general, under the cold climatic scenario, permafrost altitudinal limit extends 600 to 700 m below respect to its actual position. For instance, high permafrost likelihood under these assumptions reached 3650 m a.s.l. (current creeping permafrost limit), while medium permafrost likelihood may have descended up to 2850 m a.s.l. Moreover, permafrost surficial extension in coarse-blocky deposits, comparing present with cold climatic scenarios, display a reduction of 56%, 34% and 13% for high, medium and low likelihood permafrost categories, respectively.

Table 3. Permafrost probabilistic values, altitudinal levels and surfaces, according to the CBDP model, under the cold climatic scenario vs present climatic conditions.

Permafrost Probability	MAAT – 5°C Scenario		Present Climatic Scenario	
	(Altitude m a.s.l.)	Surface (km ²)	(Altitude m a.s.l.)	Surface (km ²)
High likelihood	>3650	2785	>4200	1200
Medium likelihood	2850 to 3650	9380	3400 to 4200	6178
Low likelihood	2300 to 2850	12.717	3000 to 3400	11.060
No Permafrost	<2300	Not calculated	<3000	Not calculated

4.5. Comparison with rock glacier inventory

The rock glacier inventory of Argentina (IANIGLA, 2017) includes only active and inactive rock glaciers, with surfaces >0.01 km² but no information regarding fossil landforms (with no permafrost or ice-rich permafrost *in situ*) is available at the moment. In the Dry Andes studied area, 3318 rock glaciers were identified by IANIGLA (2017): 2494 active and 825 inactive forms. No significative differences in altitude of fronts for active and inactive rock glaciers were found (4059 ± 265 m a.s.l. and 4007 ± 331 m a.s.l., respectively), with rock glaciers developing between 3400 and 5300 m a.s.l. From the 3318 analysed rock glaciers, 48% have their front below a MAAT of -2.75°C (high permafrost likelihood); 50% have their front between -2.75° up to 1.3°C (medium permafrost likelihood) and, 2% of the rock glaciers present their fronts with MAATs over 1.3°C (low permafrost likelihood).

According the CBDP model, 6% of the rock glaciers in the study area present high permafrost likelihood conditions, 42% medium permafrost likelihood, 38% low permafrost likelihood and, 14% of them, arguably no present permafrost conditions.

Comparing with a cold climatic scenario, permafrost occurrence probability in these bodies was: reduction of 62% in high likelihood category, reduction of 30% in medium likelihood category, increase of 75% in low likelihood category and, increase of 474% in no permafrost presence category. Regarding likely permafrost degradation occurrence, under present climatic scenario 0.9% of the rock glaciers display likely degraded permafrost patterns and 33% of them, possible degraded permafrost patterns.

5. Discussion

5.1. Permafrost extension and background data

Results achieved with our CDBP model are consistent with available background data. For example, at 28° S in the Desert Andes, the lowest altitudinal limit of mountain creeping permafrost was estimated to be 4300-4500 m a.s.l. (Barsch, 1978); while continuous in situ mountain permafrost was placed at appr. 5000 m a.s.l. (Scholl, 2002; Perucca and Éesper Angillieri, 2008). At 30° S in the Central Andes of Argentina, lowest altitude of creeping permafrost, based on the altitude of active rock glacier's toes, is at 4000 m a.s.l. according to Schrott (1996) or at 3600 m a.s.l. according to Éesper Angillieri (2009), using also the toe's altitude of inactive rock glaciers. Éesper Angillieri (2017) also calculated the permafrost extension for the study area, using an empiric statistical model with rock glaciers (active and inactive landforms) as predictive variable. This model displays a surface for high permafrost likelihood of 10.700 km², much higher than the 1200 km² calculated in this work. As the author correctly states, an overestimation of permafrost surface was arguably achieved due to the inclusion of different kind of land covers in the model and, creeping processes of rock glaciers beyond permafrost limits (Boeckli et al., 2012).

Result differences between our model and PZI values are caused by two reasons (Table 4): first, the PZI model calibration is based on the IPA map thresholds for permafrost classes (Brown *et al.*, 1997), widely used in the northern hemisphere and flat landscapes, but the CDBP model is calibrated with local data. As shown, major differences are achieved in the lower limits of probabilistic classes, with CDBP predicting permafrost presence even with positive MAATs (Table 4).

Permafrost presence with positive MAAT is a fact largely noted in the Central Andes of South America, with active and inactive rock glaciers with terminus placed near or below the 0°C isotherm (Trombotto *et al.*, 1999; Brenning, 2005; Brenning and Trombotto, 2006; Azócar *et al.*, 2017; Tapia Baldis, 2018). Our results comparing the CDBP model with Argentine rock glacier inventory (IANIGLA, 2017) also shown that the presence of active and inactive rock glaciers with positive MAAT in their front is common in the studied area. The threshold for rock glacier occurrence is 1.3°C from geomorphological data, closely to the 1.5°C limit of the medium likelihood permafrost occurrence category according the CDBP model. However, we found out that 2% of the identified rock glaciers, are placed under highly unfavourable present climatic conditions and exhibit likely degraded permafrost occurrence spatial patterns. We suspect that these cases may belong to fossil or relict landforms, with no actual permafrost presence, or were incorrectly identified as rock glaciers.

Table 4. Permafrost probabilistic values and altitudinal levels according to the PZI and the CBDP models. Corresponding MAAT values are provided in text.

Permafrost Probability	PZI Altitude (m a.s.l.)	CBDP Altitude (m a.s.l.)
High likelihood	4500 to 5100	4200 to 5700
Medium likelihood	4000 to 4500	3400 to 4200
Low likelihood	3700 to 4000	3000 to 3400
No Permafrost	3500 to 3700	1000 to 3000

The second reason to explain the differences between the CBDP and the PZI model is that the first one, exhibits broader permafrost patterns, both spatial and altitudinal, due to the different debris covers, not discriminated in the PZI model. As was previously stated, creeping permafrost landforms such as active and inactive rock glaciers, protalus ramparts and lobes, are widely used as permafrost indicators in statistic modelling methodologies. Permafrost may also appear a non-creeping phenomenon in cryoplanation surfaces and below perennial snow patches. However, some other landforms may possess permafrost under special circumstances but are not used as reliable permafrost presence indicators, such as: glacial moraines, debris and frozen-debris slopes or mass wasting deposits (Trombotto, 1991). Perennial cryotic state of permafrost may produce ground ice accretion in marginal sides of glaciers and below past-glacial covertures. Trombotto (2002) and Brenning and Trombotto (2006), stated that high permafrost probability values could also exist beneath cold glaciers because of the thermal properties of the ground are similar. These authors determine that, under a hypothetical scenario of glaciers absence or disappearance, permafrost may aggrade or grow instead. Mass wasting deposits originated or terminated in the cryogenic environment may also develop permafrost and ground-ice growth but this hypothesis has not yet been contrasted in the study area. Some general descriptions mention the presence of ice-cored moraines in the Dry Andes, that may have glacial-ice cores injected by glacio-tectonically processes and permafrost, however not exact location of these examples is provided in literature review. High probability values of permafrost occurrence were achieved for current fluvial plains. It is true that, in the calibration zone, fluvial plains are exclusively developed in the perennial freezing environment and coarse blocks carried by high-energy currents. Permafrost presence below mountain fluvial streams was suggested by Mendoza *et al.* (2016) in the Dry Andes but more detailed studies are required in order to support this statement. García *et al.* (2017), also reported differences with PZI model and geomorphological evidences of permafrost in the Dry Andes of Chile. This performance is similar to our results, and is likely due to the northern hemisphere calibration parameters used in the PZI model, that broadly differ from the existing local conditions in Dry and Central Andes of South America. Thereby, it is possible that permafrost extension in the Central Andes of South America is higher than the global PZI expectations, in concordance with geomorphological data.

5.2. Spatial patterns of permafrost degradation

Paleoclimatic reconstructions show that, since the last global glacial maximum LGM (appr. 25-20 kyr), air temperature may have been increased from 5.6° to 5.7°C in the northeast side of Chilean Andes (29° to 31°S; Kull *et al.*, 2002). According Zech *et al.* (2017), deglaciation started at appr. 18 kyr in the Dry Andes, after the LGM, at the same time with the global rise of atmospheric CO². Under these assumptions, we considered the past climatic scenario of MAAT-5°C to be equivalent to the Tardiglacial (*ca.* 18-12 kyr) conditions in the study area.

According to our results, during the transition from cold to actual climatic settings, coarse-blocky deposits in general, and rock glaciers particularly, experienced permafrost degradation, both in surface and in probabilistic occurrence values. However, the thermal response of the increase of the air temperature was arguably slow and delayed. Reasons behind this assertion are related to the thermal properties of frozen sediments in the Dry Andes (Trombotto y Borzotta, 2009); with low thermal diffusivity and conductivity ranges. In addition, the thermal balance in coarse-blocky deposits is more important during the cold than the warm periods. For example, the lack of a thick snow cover in the Dry Andes during winter, allows the no-inhibition of the cooling effect due to convective air circulation. Therefore, ground below coarse-blocky deposits stay under active freezing conditions along all year. This behaviour could have acted similar under longer-time periods, such as the transition from Tardiglacial (*ca.* 18-12 kyr) to current climatic conditions, if precipitation rates remain slow in the Central and Dry Andes. Trombotto and Borzotta (2009) also suggests that, if sediment supply remains active, thermal mechanisms may remain in time and permafrost arguably persist, even under warmer climatic scenarios.

For instance, Figure 5 display the differences in permafrost occurrence patterns in two rock glaciers from the Bramadero river basin. Example a) is an active rock glacier placed at 31.53°S and 70.11°W, frontal toe at 3920 m a.s.l. and root at 4220 m a.s.l. Example b) is an inactive rock glacier placed at 31.91°S and 70.15°W, frontal toe at 4000 m a.s.l. and root at 4600 m a.s.l. In Figure 5a, the core of a rock glacier shows high permafrost likelihood in the centre, where the deformation-creep processes are more active, according to the morphological features. In the transition towards a warmer climatic scenario (present climate), the permafrost core remains with lower probabilities of occurrence. Major reductions of permafrost are expected in northwest sides of the rock glacier and in the rooting area. However, the Figure 5b shows an inactive rock glacier placed 3.5 km east of the first example, with the same orientation but a higher front. In this case, two separated cores of likely permafrost remain since Tardiglacial scenario, one in the rooting area and the other one placed in the middle of the landform. Nevertheless, the remain area express unlikely permafrost occurrence nowadays. Geomorphological features, such as a debris flow gully coming from the rock glacier's toe, may indicate a thickening of the active layer and increase in water content. However, specific studies for such kind of processes should be addressed by landform example, as may also reflect local hydrological behaviour.

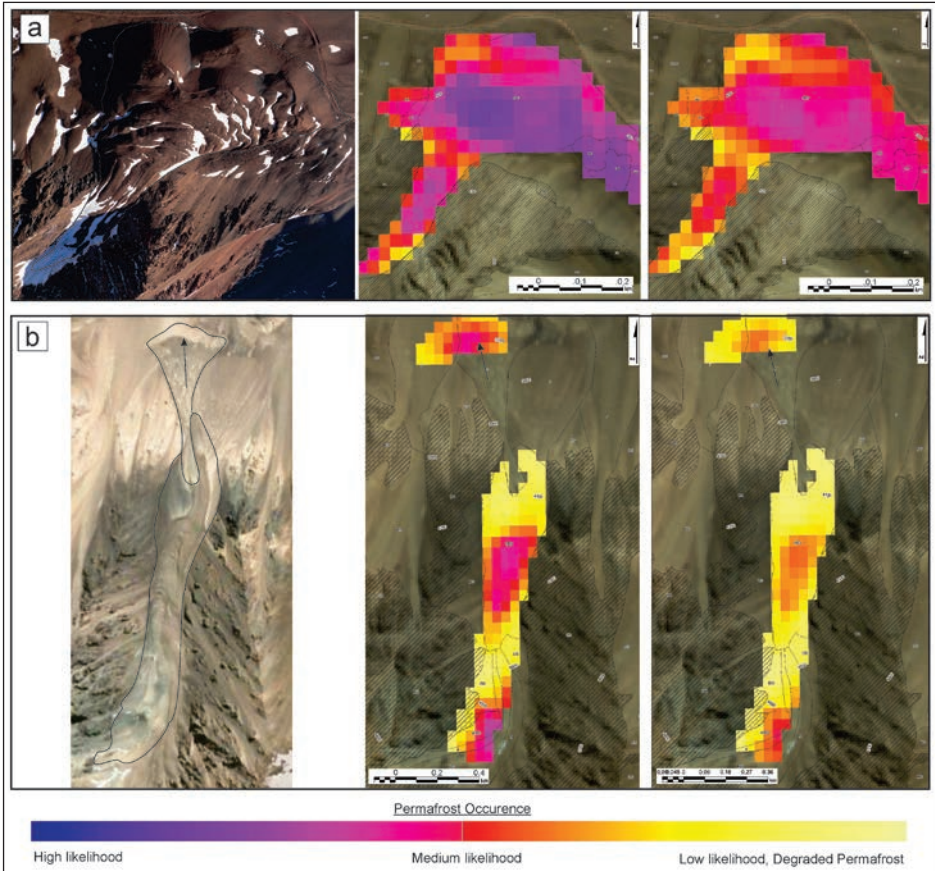


Figure 5. Reduction of permafrost probability according to CBDP model, from a “cold climatic scenario” to present climatic conditions. In both examples, central picture represents the cold scenario and the right picture, the occurrence under the present climate scenario. a) Active rock glacier placed at 31.53°S and 70.11°W , frontal toe at 3920 m a.s.l. and root at 4220 m a.s.l. (Photo: GGGNCC, 2016). Example b) Inactive rock glacier placed at 31.91°S and 70.15°W , frontal toe at 4000 m a.s.l. and root at 4600 m a.s.l. (Base figure: ALOS-PRISM imagery).

Regarding warming climatic scenarios, Drewes *et al.* (2018) recently predicted that under the RCP 8.5 extreme warming climatic scenario, the 0°C isotherm may be rise-up 500 m in the Central Andes of Argentina, leading to a situation where 95% of current active and inactive rock glaciers will be placed below over regions with positive MAATs. Osterkamp (2007) showed that temperature and extension of permafrost are very sensitive to climatic changes but their response may be complex and heterogeneous. In several regions around the world, permafrost temperatures have been raising during the last decades, but some places show no temperature change while in others, contrary, permafrost temperature has decreased (Romanovsky *et al.*, 2010).

Temperature increase is marked in cold permafrost areas but no over warmer permafrost, the last one arguably expected in the Dry Andes. In ice-rich warmer permafrost, heat is used to partially melt the ground ice thus, buffering ground temperature increase and consequently, ice melting. Nevertheless, more studies are needed and thermal response of material should also be included in all previous assumptions, as well as ground-ice volumetric estimation and thermal state of permafrost. First results of ice volumetric estimation in the Dry Andes were recently presented by Halla *et al.* (2018). In addition, changes in precipitation patterns may play a significative part in regional patterns of permafrost distribution, controlling the timing and thickness of snow cover.

5.3. CBDP limitations

The spatial resolution of the CBDP model is limited by the pixel size of AR-DEM; its extension is restricted from 28° to 33°S and 70°30' to 69°W. The CBDP model responds only to the specific calibration data set and may not perform well for extrapolation to other spatial-temporary conditions. Further, displayed maps of permafrost maps have predictive and no-explanatory behaviour. In other words, the CBDP model may be useful to identify regional patterns of spatial occurrence, but it does not consider the local influence of ground thermal properties or snow timing, thickness and duration, properties that could also affect the thermal permafrost state.

By using NCEP-CSFR air temperature gridded data, local climatic processes may eventually not be expressed or visualized. Besides, while computing the MAAT for the 1979-2010 period a “mean climatic present scenario” is achieved, neglecting the warming or cooling periods. This leads to an optimistic estimation, biased towards an overestimation of permafrost distribution. The use of the standard air temperature lapse rate (-6.5°C/1000 m) even though it is an oversimplification for the MAAT calculation and may not reflect local lapse rates, could be accepted as mean value in long-time reconstructions, as stated by Shauwecker *et al.* (2011). Besides, Zou *et al.* (2017) correctly stated that MAAT may be an inadequate predictor of ground surface temperature (GST), and pointed out several alternatives to estimate GST over larger areas with no *in situ* data. Nevertheless, no sufficient number of measurements are available in the study area to calibrate a permafrost model with GST data and, even under these assumptions, biased results may be achieved (Zou *et al.*, 2017).

The discrimination between steep bedrock and surfaces of coarse-blocky deposits was previously made by (Gruber and Haeberli, 2009; Brenning and Trombotto, 2006; Boeckli *et al.*, 2012, Azócar *et al.*, 2017; Deluigi *et al.*, 2017), using slope ranges from 35° to 37°. In our findings, high ruggedness steep slopes (TRI values >19-20) were excluded from the CBDP model as permafrost prone areas; however, we need to state that these kinds of slopes may have permafrost state, expressed as ice among rock fractures. In addition, some bedrock areas with TRI values <19-20 were automatically considered as coarse-debris deposits, thus displaying high permafrost occurrence likelihood. Needless to say, that the CBDP model should be complemented by a statistical model for permafrost distribution in rock outcrops. Permafrost probability in intact, fractured or weathered rocks should be calculated using the ground

temperature, thermal properties of the rocks, weathering degree, mechanical state of the rock massif and distribution of snow cover (besides its distribution by wind blows and snow avalanches). According to Boeckli *et al.*, (2012), fractured rock surfaces enhance snow accumulation, moreover water percolation and advection through snow melting followed by water refreezing, locally may contribute for cryotic conditions to sustain. For instance, seasonal ice veins in fractures and caves from 4000 m a.s.l. and on south exposed slopes were directly observed in the study area. On the other hand, steep slopes with coherent rocks, locally exposed to higher solar radiation rates, not only complicate the snow pack accumulation but also display higher ground surficial temperatures. The lack of equipment and the remoteness of the study area, hamper the achievement of such kind of model at this moment.

6. Conclusions

The study presents a statistical model to display the permafrost presence likelihood over coarse-blocky surfaces in the Dry Andes of Argentina, from 28° to 33°S. High permafrost likelihood in the study area is expected between 4200 and 5700 m a.s.l., from south to north and covers a surface of approximately 1200 km². Medium permafrost likelihood is expected between 3400 and 4200 m a.s.l. with a surface of 6178 km² while low permafrost likelihood, occurs between 3000 and 3400 m a.s.l. with an area of 11.060 km². The results showed that landforms composed by coarse-blocky deposits may also have, such as: frozen talus slopes, glaciers and covered glaciers, moraines and morainic complexes, rock avalanches and rock slides. However, permafrost presence should be confirmed by geophysical prospecting over such kind of debris deposits in the Dry Andes and in situ installation of ground temperature recording, in order to establish the thermal state of permafrost. Even though the CBDP model may be useful to identify the regional patterns of permafrost occurrence, it should not be used in an explanatory sense, as it does not consider the local influence of ground thermal characteristics or snow timing and thickness, properties that could also affect the thermal permafrost state. Moreover, it does not reflect the ice presence in the ground. Permafrost absence should also be determined, in order to avoid surficial overestimations.

Our model was used to estimate the extension of permafrost in past climatic scenarios and spatial patterns of areas with arguably degradation processes. An inventory of permafrost degradation features in the sense of the work presented by Marcer *et al.* (2019), corroborated with field data, could be used in order to contrast and improve our findings. We propose a picture in which permafrost surficial extension in coarse-blocky deposits, comparing present with cold climatic scenarios, displays a reduction from 13% to 56% in all the probabilistic categories. Besides, 14% of the geomorphologically classified active and/or inactive rock glaciers display unlikely permafrost occurrence under the present climatic conditions.

Future work will focus on the integration of thermal ground parametrization in coarse-blocky surfaces and, the integration with a statistical model for permafrost distribution in rock outcrops.

Acknowledgements

This study is part of the PhD thesis of C. Tapia Baldis (2018, Unpublished). It was funded by the project PIP 1222015-0100913 (2015-2017) under the direction of Dr Dario Trombotto. Authors express their gratitude to Martín Mendoza, Ivanna Pecker, Pablo Gutiérrez and José Hernández for their valuable help during field tasks; and the Gabinete de Geocirología, Glaciología, Nivología y Cambio Climático (GGNCC) de la FCEFYN-UNSJ for photo permissions. We thank to the anonymous reviewers and the GRL editors for constructive criticism and thoughtful reviews, which greatly improved our study. The datasets generated during the current study are available from the corresponding author on reasonable request.

References

- Akaike, H. 1974. A new look at the statistical model identification. *IEEE Transaction on Automatic Control* 19 (6), 716-723.
- Arenson, L.U., Pastore, S., Trombotto, D., Bolling, S., Quiroz, M.A., Ochoa, X.L. 2010. Characteristics of two rock glaciers in the dry Argentinean Andes based on initial surface investigations. *Proceedings 6th Canadian Permafrost Conference*, Calgary, Alberta.
- Azócar, G.F., Brenning, A. 2010. Hydrological and Geomorphological Significance of Rock Glaciers in the Dry Andes, Chile (27°-33°S). *Permafrost and Periglacial Processes* 21, 41-53. <https://doi.org/10.1002/ppp.669>.
- Azócar, G.F., Brenning, A., Bodin, X. 2017. Permafrost distribution modelling in the semi-arid Chilean Andes. *The Cryosphere* 11, 877-890. <https://doi.org/10.5194/tc-11-877-2017>.
- Balch, E.S. 1900. *Glacieres, or freezing caverns*. Allen Lane and Scott, Philadelphia.
- Barsch, D. 1978. Active rock glaciers as indicators of discontinuous permafrost: an example from the Swiss Alps. *Proceedings 3rd International Conference on Permafrost*, Ottawa, pp. 349-352.
- Barsch, D. 1996. *Rock glaciers. Indicators for the present and former geo-ecology in high mountain environment*. Springer-Verlag, Heidelberg, 331 pp.
- Boeckli, A., Brenning, A., Gruber, S., Noetzli, J. 2012. A statistical approach to modelling permafrost distribution in the European Alps or similar mountain ranges. *The Cryosphere* 6 (1), 125-140. <https://doi.org/10.5194/tc-6-125-2012>.
- Brenning, A. 2005. Geomorphological, hydrological and climatic significance of rock glaciers in the Andes of central Chile (33-35°S). *Permafrost and Periglacial Processes* 16 (3), 231-240. <https://doi.org/10.1002/ppp.528>.
- Brenning, A., Trombotto, D. 2006. Logistic regression modeling of rock glacier and glacier distribution: Topographic and climatic control in the semi-arid Andes. *Geomorphology* 81, 141-154. <https://doi.org/10.1016/j.geomorph.2006.04.003>.
- Brown, J., Christiansen H.H., Ferrians, O.J., Heginbottom, J.A., Melnikov, E.S. 1997. *Circum-arc map of permafrost and ground ice conditions*. U.S. Geological Survey Circum-Pacific Map Series, CP-45, 1 sheet, scale 1:10 000 000. <http://nsidc.org/data/index.html>.
- Cao, B., Gruber, S., Zhang, T. 2017. REDCAPP (v1.0): Parameterizing valley inversions in air temperature data downscaled from re-analyses. *Geoscientific Model Development* 10, 2905-2923. <https://doi.org/10.5194/gmd-10-2905-2017>.
- Croce, F., Milana, J.P. 2002. Internal structure and behavior of a rock glacier in the arid Andes of Argentina. *Permafrost and Periglacial Processes* 13, 289-299. <https://doi.org/10.1002/ppp.431>.

- Delaloye, R., Lambiel, C. 2005. Evidence of winter ascending air circulation throughout talus slopes and rock glaciers situated in the lower belt of alpine discontinuous permafrost (Swiss Alps). *Norwegian Journal of Geography* 59 (2), 194-203. <https://doi.org/10.1080/00291950510020673>.
- Delaloye, R., Reynard, E., Lambiel, C. 2003. Pergélisol et construction de remonteés mécaniques: l'exemple des Lapires (Mont-Gelé, Valais), Frost in der Geotechnik. *Mitteilungen der Schweizerischen Gesellschaft für Boden- und Felsmechanik*, 141, 103-113.
- Deluigi, N., Lambiel, C., Kanevski, M. 2017. Data-driven mapping of the potential mountain permafrost distribution. *Science of the Total Environment* 590-591, 370-380. <https://doi.org/10.1016/j.scitotenv.2017.02.041>.
- Drewes, J., Moreiras, S., Korup, O. 2018. Permafrost activity and atmospheric warming in the Argentinian Andes. *Geomorphology* 323, 13-24. <https://doi.org/10.1016/j.geomorph.2018.09.005>.
- Ésper Angillieri, Y. 2009. A preliminary inventory of rock glaciers at 30° S latitude, Cordillera Frontal of San Juan, Argentina. *Quaternary International* 195, 151-157. <https://doi.org/10.1016/j.quaint.2008.06.001>.
- Ésper Angillieri, M.Y. 2017. Permafrost distribution map of San Juan Dry Andes (Argentina) based on rock glacier sites. *Journal of South American Earth Sciences* 73, 42-49. <https://doi.org/10.1016/j.jsames.2016.12.002>.
- García, A., Ulloa, C., Amigo, G., Milana, J.P. 2017. An inventory of cryospheric landforms in the arid diagonal of South America (high Central Andes, Atacama region, Chile). *Quaternary International* 438, 4-19. <http://dx.doi.org/10.1016/j.quaint.2017.04.033>.
- Gruber, S. 2012. Derivation and analysis of a high-resolution estimate of global permafrost zonation. *The Cryosphere* 6 (1), 221-223. <https://doi.org/10.5194/tc-6-221-2012>.
- Gruber, S., Hoelzle, M. 2008. The cooling effect of coarse blocks revisited: a modeling study of a purely conductive mechanism. In: D.L. Kane, K.M. Hinkel (Eds.), *Proceedings of the 9th International Conference of Permafrost*, Institute of Northern Engineering, Fairbanks, AK, pp. 581-586.
- Gruber, S., Haeblerli, W. 2009. Mountain permafrost. In: R. Magesin, R. (Ed.), *Permafrost soils*. Springer, Berlin, 33-34. https://doi.org/10.1007/978-3-540-69371-0_14.
- Haeblerli, W. 1985. Creep of mountain permafrost: internal structure and flow of alpine rock glaciers. *Mitteilungen Versuchsanstalt für Wasserbau, Hydrologie und Glaziologie*, ETH Zürich, 77, 1-142.
- Haeblerli, W., Noetzli, J., Arenson, L., Delaloye, R., Gärtner-Roer, I., Gruber, S., Isaksen, K., Kneisel, C., Krautblatter, M., Phillips, M. 2010. Mountain permafrost: development and challenges of a young research field. *Journal of Glaciology* 56, 1043-1058. <https://doi.org/10.3189/002214311796406121>.
- Halla, C., Blöthe, J.K., Tapia Baldis, C., Hauck, C., Schrott, L. 2018. Volumetric ice content in active rock glaciers derived from geophysical modelling (Central Andes of Argentina). *Book of Abstracts, EUCOP 5*, Chamonix Mont-Blanc, pp. 886-887.
- Harris, C., Arenson, L., Christiansen, H.H. et al. 2009. Permafrost and climate in Europe: Monitoring and modelling thermal, geomorphological and geotechnical responses. *Earth-Science Reviews* 92, 117-171. <https://doi.org/10.1016/j.earscirev.2008.12.002>.
- Hoelzle, M., Haeblerli, W. 1995. Simulating the effects of mean annual air temperature changes on permafrost distribution and glacier size: An example from the Upper Engadin, Swiss Alps. *Annals of Glaciology* 21, 399-405. <https://doi.org/10.3189/S026030550001613X>
- Hosmer, D. W. and Lemeshow, S. 2000. *Applied logistic regression*. John Wiley & Sons, Biosphere Reserves. UNESCO, Paris, pp. 28-39.

- Humlum, O. 1996. Origin of rock glaciers: observations from Mellemfjord, Disko Island, central West Greenland. *Permafrost and Periglacial Processes* 7 (4), 361-380.
- IANIGLA, 2017. *Inventario nacional de glaciares*. CONICET MENDOZA. Url: <http://www.glaciaresargentinos.gov.ar> (Accessed November 2017).
- Isacks, B., Jordan, T.E., Allmendiger, R.W., Ramos, V.A. 1982. La segmentación tectónica de los Andes Centrales y su relación con la Placa de Nazca subductada. *V Congreso Latinoamericano de Geología*, Actas III, pp. 587-606. Buenos Aires.
- Johansen, O. 1975. *Thermal conductivity of soils*. Ph.D. Thesis, Trondheim, Norway. (CRREL Draft Translations 637, 1977).
- Jordan, T.E., Isacks, B.L., Allmendiger, R.W., Brewer, J.A., Ramos, V.A., Ando, C.J. 1983. Andean tectonics related to geometry of subducted Nazca Plate. *Geological Society of America, Bulletin* 94 (3), 341-361. [https://doi.org/10.1130/0016-7606\(1983\)94<341:ATRGTGO>2.0.CO;2](https://doi.org/10.1130/0016-7606(1983)94<341:ATRGTGO>2.0.CO;2).
- Juliussen, H., Humlum, O. 2008. Thermal regime of openwork block fields on the mountains Elgåhogna and Sølén, central-eastern Norway, *Permafrost and Periglacial Processes* 19, 1-18. <https://doi.org/10.1002/ppp.607>.
- Kleinbaum, D.G., Klein, M. 2010. *Logistic regression. A self-learning text*. Third edition. Springer, New York, Dordrecht, Heidelberg, London, 702 pp.
- Kull, C., Grosjean, M., Veit, H. Modeling Modern and Late Pleistocene Glacio-Climatological Conditions in the North Chilean Andes (29-30°). *Climatic Change* 52, 359-381. <https://doi.org/10.1023/A:1013746917257>.
- Liboutry, L. 1998. Glaciers of Wet Andes. In: W.M.J. Ferrigno (Ed.), *Satellite image atlas of glaciers of the world*. US Government Printing Office, Washington DC, pp. 109-206.
- Martini, M.A., Strelin, J.A., Astini, R.A. 2013. Inventario y caracterización morfoclimática de los glaciares de roca en la Cordillera Oriental argentina (entre 22° y 25° S). *Revista Mexicana de Ciencias Geológicas* 30 (3), 569-581.
- Mendoza, M., Villarreal, C.D., Tapia Baldis, C., Forte, A.P., Gianni, R., Krusse, E. 2016. Aspectos hidrológicos del ambiente periglacial en la cuenca del Río Santa Cruz, provincia de San Juan. *Actas del IX Congreso Argentino de Hidrogeología*, San Fernando del Valle de Catamarca, Argentina, 197- 204.
- Marcet, M., Bodin, X., Brenning, A., Schoeneich, P., Charvet, R., Gottardi, F. 2017. Permafrost favorability index: Spatial modeling in the French Alps using rock glacier inventory. *Frontiers in Earth Science* 5, 1-17. <https://doi.org/10.3389/feart.2017.00105>.
- Marcet, M., Serrano, C., Brenning, A., Bodin, X., Goetz, J., Schoeneich, P. 2019. Evaluating the destabilization susceptibility of active rock glaciers in the French Alps. *The Cryosphere* 13, 141-155. <https://doi.org/10.5194/tc-13-141-2019>
- Montecinos, A., Aceituno, P. 2003. Seasonality of the ENSO-related rainfall variability in the Central Chile and associated circulation anomalies. *Journal of Climate* 16, 281-296. [https://doi.org/10.1175/1520-0442\(2003\)016<0281:SOTERR>2.0.CO;2](https://doi.org/10.1175/1520-0442(2003)016<0281:SOTERR>2.0.CO;2).
- Osterkamp, T.E. 2007. Characteristics of the recent warming of permafrost in Alaska. *Journal of Geophysical Research-Earth Surface* 112, 10 (F02S02). <https://doi.org/10.1029/2006JF000578>.
- Perucca, L.P., Éspér Angillieri, M.Y. 2008. A preliminary inventory of periglacial landforms in the Andes of La Rioja and San Juan, Argentina, at about 28° S. *Quaternary International*, 190, 171-179. <https://doi.org/10.1016/j.quaint.2007.10.007>.
- Ramos, V.A., Cegarra, M., Lo Forte, G., Comínguez, A. 1997. El frente orogénico en la Sierra de Pederal (San Juan, Argentina): su migración a través de los depósitos orogénicos. *Actas VIII Congreso Geológico Chileno* 3, 1709-1713. Antofagasta, Chile.

- Riseborough, D., Shiklomanov, N., Etzelmüller, B., Gruber, S., Marchenko, S. 2008. Recent advances in permafrost modelling. *Permafrost and Periglacial Processes* 19 (2), 137-156. <https://doi.org/10.1002/ppp.615>.
- Ryley, S.J., DeGloria, S.D., Elliot, R. 1999. A terrain ruggedness index that quantifies topographic heterogeneity. *Intermountain Journal of Sciences* 5, 23-27.
- Romanovsky, V.E., Smith, S.L., Christiansen, H.H. 2010. Permafrost thermal state in the Polar Northern Hemisphere during the International Polar Year 2007-2009: A Synthesis. *Permafrost and Periglacial Processes* 21, 106-116. <https://doi.org/10.1002/ppp.689>.
- Saha, S., Moorthi, H., Pan, X., et al. 2010. *NCEP Climate Forecast System Reanalysis (CFSR) 6-hourly Products, January 1979 to December 2010*. Research Data Archive at the National Center for Atmospheric Research, Computational and Information Systems Laboratory. <https://doi.org/10.5065/D69K487J> (Accessed 02 november 2015).
- Saito, K., Trombotto Liaudat, D., Yoshikawa, K., Mori, J., Sone, T., Marchenkon, S., Romanovsky, V., Walsh, J., Hendricks, A., Bottegal, E. 2016. Late Quaternary permafrost distributions downscaled for South America: Examinations of GCM-based maps with observations. *Permafrost and Periglacial Processes* 27, 43-55. <https://doi.org/10.1002/ppp.1863>.
- Sattler, K., Anderson, B., Makintosh, A., Norton, K., de Róiste, M. 2016. Estimating permafrost distribution in the maritime Southern Alps, New Zealand, based on climatic conditions at rock glacier sites. *Frontiers in Earth Science* 4 (4), 1-17. <https://dx.doi.org/10.3389/feart.2016.00004>.
- Schauwecker, S., Pellicciotti, F., McPhee, J. 2011. Near-surface temperature lapse rates in a mountainous catchment in the Chilean Andes. *Proceedings from AGU Fall Meeting*, San Francisco, California, USA.
- Scherler, M., Schneider, S., Hoelzle, M., Hauck, C. 2014. A two-sided approach to estimate heat transfer processes within the active layer of the Muertèl-Corvatsch rock glacier. *Earth Surface Dynamics* 2, 141-154. <https://doi.org/10.5194/esurf-2-141-2014>.
- Scholl, K.H. 2002. Geomorphological mapping of the periglacial level in the Semiarid Andes. In: D. Trombotto, D., R. Villalba (Eds.), *IANIGLA, 30 años de investigación básica y aplicada en ciencias ambientales*, IANIGLA-CONICET, Mendoza, 269 pp.
- Schrott, L. 1996. Some geomorphological – hydrological aspects of rock glaciers in the Andes (San Juan, Argentina). *Zeitung für Geomorphologie* 104, 161-173.
- Tapia Baldis, C. 2018. *Distribución y características del ambiente periglacial en el extremo oeste del departamento Calingasta, Provincia de San Juan, Argentina*. Tesis Doctoral, Universidad Nacional de San Juan (Inédita), San Juan, 390 pp.
- Trombotto, D. 1991. Untersuchungen zum periglazialesn Formenschatz und zu periglazialen Sedimenten in der “lagunita del Plata”, Mendoza, Argentinien. *Heidelberger Geographische Arbeiten* 90, 171 pp.
- Trombotto, D. 2000. Survey of cryogenic processes, periglacial forms and permafrost conditions in South America. *Revista do Instituto Geológico Sao Paulo*, 21 (1-2), 33-55.
- Trombotto, D. 2002. El ambiente criogénico actual y el paleopermafrost en el extremo austral de América del Sur. In: D. Trombotto, D., R. Villalba (Eds.), *IANIGLA, 30 años de investigación básica y aplicada en ciencias ambientales*, IANIGLA-CONICET, Mendoza, 269 pp.
- Trombotto, D. 2003. Mapping of permafrost and the periglacial environment, Cordón del Plata, Argentina. *Proceedings of the 8th International Conference on Permafrost*. Zürich, pp. 161-162.
- Trombotto, D., Borzotta, E. 2009. Indicators of present global warming through changes in active layer-thickness, estimation of thermal diffusivity and geomorphological observations in the Morenas Coloradas rockglacier Central Andes of Mendoza, Argentina. *Cold Regions Science and Technology* 55, 321- 330. <https://doi.org/10.1016/j.coldregions.2008.08.009>.

- Trombotto, D., Buk, E., Hernández J. 1997. Monitoring of mountain permafrost in the Central Andes, Cordón del Plata, Mendoza, Argentina. *Permafrost and Periglacial Processes* 8, 123-129. [https://doi.org/10.1002/\(SICI\)1099-1530\(199701\)8:1<123::AID-PPP242>3.0.CO;2-M](https://doi.org/10.1002/(SICI)1099-1530(199701)8:1<123::AID-PPP242>3.0.CO;2-M).
- Trombotto, D., Buk, E., Hernández, J. 1999. Rock glaciers in the southern Central Andes (approx. 33° - 34° S), Cordillera Frontal, Mendoza, Argentina. *Bamberger Geographische Schriften* 19, 145-173.
- Trombotto Liaudat, D., Wainstein, P., Arenson, L.U. 2014. *Guía Terminológica de la Geocriología Sudamericana*, Vazquez Mazzini Editores, Mendoza, 127 pp.
- Unidad de Geocriología, 2009-2014. *Monitoreo geocriológico valle del Pachón y zonas cercanas, San Juan, Argentina*. (Unpublished Technical Report).
- Van Everdingen, R. 1998. *Multi-language Glossary of Permafrost and Related Ground-Ice Terms*, National Snow and Ice Data Center. World Data Center for Glaciology, Boulder, Colorado.
- Villarroel, C.D., Tamburini Beliveau, G., Forte, A.P., Monserrat, O., Morvillo, M. 2018. DInSAR for a Regional Inventory of Active Rock Glaciers in the Dry Andes Mountains of Argentina and Chile with Sentinel-1 Data. *Remote Sensing* 10 (10), 1588. <https://doi.org/10.3390/rs10101588>.
- Wicky, J. and Hauck, C. 2017. Numerical modelling of convective heat transport by air flow in permafrost talus slopes. *The Cryosphere* 11, 1311-1325. <https://doi.org/10.5194/tc-11-1311-2017>.
- Zech, J., Terrizzano, C., García-Morabito, E., Veit, H., Zech, R. 2017. Timing and extent of late Pleistocene glaciation in the arid Central Andes of Argentina and Chile (22°-41°S). *Cuadernos de Investigación Geográfica / Geographical Research Letters* 43 (2), 697-718. <http://doi.org/10.18172/cig.3235>.
- Zhao, S.P., Nan, Z.T., Huang, Y.B., Zhao, L. 2017. The Application and evaluation of simple permafrost distribution models on the Qinhai-Tibet Plateau. *Permafrost and Periglacial Processes* 28 (2), 391-404. <https://doi.org/10.1002/ppp.1939>.
- Zou, D., Zhao, L., Sheng, Y. *et al.* 2017. A new map of permafrost distribution on the Tibetan Plateau. *The Cryosphere* 11, 2527-2542. <https://doi.org/10.5194/tc-11-2527-2017>.